

Article

Origin of Fluoride and Arsenic in the Main Ethiopian Rift Waters

Gianluca Bianchini ¹, Valentina Brombin ^{1,*}, Chiara Marchina ², Claudio Natali ³,
Tewodros Rango Godebo ⁴, Alessandro Rasini ¹ and Gian Marco Salani ¹

¹ Department of Physics and Earth Sciences, University of Ferrara, 44122 Ferrara, Italy; bncglc@unife.it (G.B.); alessandro.rasini@socotec.com (A.R.); slngmr@unife.it (G.M.S.)

² Department of Land, Environment, Agriculture and Forestry, University of Padua, 35020 Padua, Italy; chiara.marchina@unipd.it

³ Department of Earth Sciences, University of Florence, 50121 Florence, Italy; claudio.natali@unifi.it

⁴ Department of Environmental Health Sciences, Tulane University, New Orleans, LA 70112, USA; tgodebo@tulane.edu

* Correspondence: brmvnt@unife.it

Received: 3 April 2020; Accepted: 16 May 2020; Published: 18 May 2020



Abstract: In the Main Ethiopian Rift (MER) area, rural populations often use water that exceeds the World Health Organization thresholds for fluoride (F⁻) and arsenic (As), two elements that are hazardous for human health. In this study, twenty-nine water samples were collected from lakes and hot and cold springs in southern MER to investigate source(s) and health-risk of the F⁻ and As contamination. According to major ion and trace element analyses, only cold spring water is safe for consumption, whereas hot spring water is the most contaminated. Leaching tests performed with the MER rhyolitic volcanic rocks and their weathered products (fluvio-lacustrine sediments) demonstrate that the main cause of the F⁻ and As release is geogenic, i.e., not related to anthropogenic activities. The weathering of volcanic glass and minerals (apatites, clays, hydro-oxides) by CO₂-bearing alkaline water induces the mobilisation of F⁻ and As from solid to liquid phase. This process is particularly fast, when fluvio-lacustrine sediments are involved, and can be further enhanced by hot groundwater leaching. This study, investigating the distribution, sources, and mechanisms of F⁻ and As release in MER water, could be of interest also for other sectors of the East African Rift and other similar volcano-tectonic settings.

Keywords: fluoride and arsenic; Main Ethiopian Rift; water–rock interaction; weathering; tolerance limit; geogenic contamination

1. Introduction

Groundwater is the major source of drinking water for over half of the global population [1]; however, its quality can be compromised by natural geogenic contaminants such as fluoride (F⁻) and arsenic (As). In some cases, groundwater interacts with F⁻ and As-enriched host aquifers, which releases these elements in levels that are hazardous for the human health [2]. The guideline values established by the World Health Organization (WHO) for F⁻ and As in drinking water are 1.5 mg/L and 10 µg/L, respectively [3]. Prolonged ingestion of drinking water containing concentrations of F⁻ exceeding the tolerance limit can cause dental and skeletal fluorosis, and excess of As exposure can cause skin disorders, respiratory problems, and cancer [2,4]. Therefore, F⁻ and As contamination represents a serious health issue, especially in rural communities that receive water from groundwater wells without testing for the presence of toxic contaminants (e.g., Bangladesh and India [5–7]).

While anthropogenic sources (such as pesticides, fertilizers, and soil amendments) may introduce F⁻ and As into the environment [8,9], the most common sources of F⁻ and As in groundwater are

geogenic processes. The co-occurrence of F and As in groundwater is generally associated with volcanic rocks [10–12], and these elements are ubiquitous in high-temperature geothermal settings [10,11,13]. They are commonly found in geothermal fluids, fumarolic gases, and volcanic emissions, which affect the adjacent environments (aquifers, surface water bodies, and soils [14]). Fluoride- and As-enriched groundwater is associated with geothermal activity along convergent plate boundaries (e.g., the Andes and Himalayas [15]), as well as in intraplate areas characterised by extensional tectonic activity [16–19], especially where a continental rifting phase follows the upraising of a mantle plume (e.g., the Main Ethiopian Rift [16–24]). The concentration and mobilisation of F⁻, As, and other elements associated with geothermal fluids are dependent on chemical and physical processes that occur between groundwater and its geological environment [8,10–13]. In particular, F⁻ and As behave as incompatible elements during magmatic processes, as they do not easily fit into the crystal structure of minerals and are preferentially partitioned into melt, remaining in the residual magma until its crystallisation. Therefore, F⁻ and As are more concentrated in evolved sialic rocks (e.g., rhyolites) rather than in primitive basic rocks (e.g., basalts) [13]. Accordingly, the concentrations of F⁻ and As are higher in waters that leach sialic rocks (e.g., water in Mexico [10,11]) as compared to water leaching basic rocks (e.g., water in Iceland [25]). In fact, various primary mineral phases commonly recorded in sialic rocks, such as fluorite, apatite, amphibole, biotite, and volcanic glass contain F⁻ and As [8,10–12,26–30]. Moreover, F⁻ and As are adsorbed by secondary minerals, such as Fe-, Al-, and Mn-oxides and hydroxides, and clay [10,11,16–19,31]. Other geochemical factors, such as pH and temperature, strongly affect silica dissolution and adsorption–desorption reactions in secondary minerals during rock weathering [12]. The processes are enhanced in alkaline conditions, especially in arid/semi-arid dry climates that favour F⁻ and As mobilisation and release into groundwater [10,11,16–19,31]. In several studies, similar geological, geochemical, and environmental conditions have been identified as key source of F⁻ and As co-contamination in aquifers (e.g., Mexico and Argentina [10,11,32]). In rift zones (e.g., in Namibia and Madagascar [33,34]) the release of F⁻ and As in circulating groundwater is also enhanced by the presence of active faults promoting the influx of endogenic CO₂ from the mantle source, which facilitates the dissolution of silicates and oxides and hydroxides.

Elevated F⁻ and As concentrations were found also in another rift system, the Main Ethiopian Rift (MER), which is part of the East African Rift valley system [19,35]. The MER is the most populated area of Ethiopia (density of population: 250–350 people km⁻²), and the majority of people (84%) lives in rural zones practicing agriculture. In MER, the water supplies are mainly represented by groundwater wells. However, several works have emphasised that up to 8 million people living in the MER are at risk from exposure to high levels of F⁻ and As in the groundwater [16–19,36–40]. Considering that anthropogenic contamination is very low in MER water (as demonstrated by the very low contents of nitrate and sulphate), it is plausible to assume that the co-occurrence of F⁻ and As is also not related to human activities and has to be considered geogenic [40]. Unfortunately, despite the awareness of the F⁻ and As problem, rural communities have relatively limited alternatives to using wells for drinking, and the use of water treatment to remove contaminants is rare [37]. According to Rango et al. [16–19,37,38], MER water use is causing severe deterioration of teeth and bone quality (e.g., dental and skeletal fluorosis) in the local populations, especially in young people [37–39], whereas effects related to As exposure are still not manifested in the MER region. However, in other study cases, such as in Latin America regions, the co-occurrence of F⁻ and As in groundwater is currently being monitored as it could be responsible for both dental and skeletal fluorosis and Endemic Regional Chronic Hydroarsenicism (skin lesions [4]), as well as for reducing IQ levels and decreasing intellectual functionality in children [10].

The present work investigates the quality of groundwater in the southern MER sector (i.e., the Awasa, Abaya, and Chamo lakes area; Figure 1), which was not investigated thoroughly in previous studies. In particular, this work presents new geochemical analyses of:

- (1) Lake and hot and cold spring waters (preliminarily studied by Belete et al. [26]);
- (2) Bulk rocks and constituent minerals of MER aquifer matrices;

- (3) Leachates obtained from water extraction tests with the MER rhyolitic volcanic rocks and fluvio-lacustrine sediments, performed to simulate the water–rock interaction processes in the area.

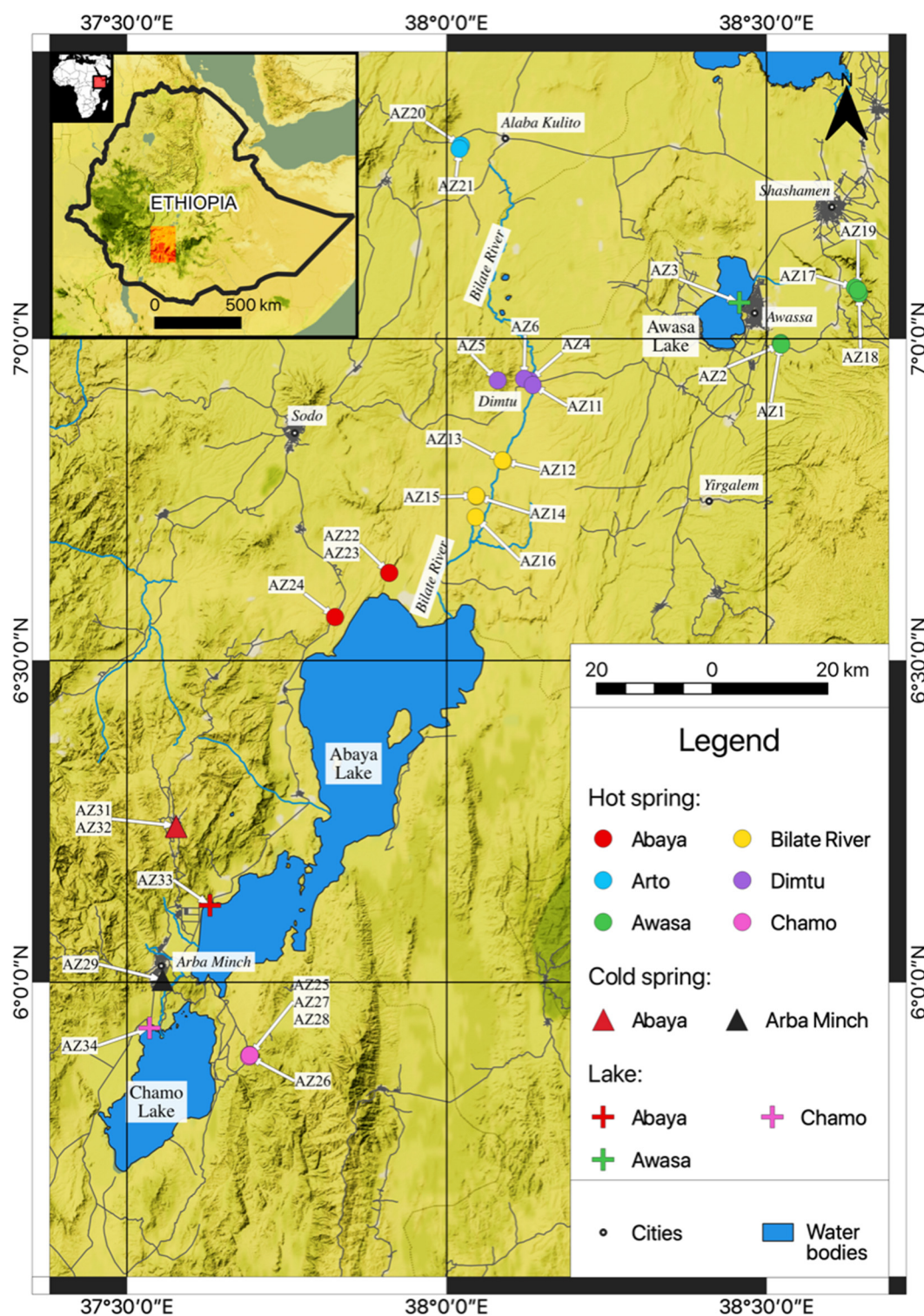


Figure 1. Sampling locations of lakes and hot and cold springs in the Awasa-Abaya-Chamo lakes district in the southern Main Ethiopian Rift (MER).

The new data, integrated with those from previous investigations, allow a comprehensive discussion on the origin and geochemical processes that ultimately lead to the MER water geochemistry.

2. Geological Setting

The MER valley is a large tectonic basin that constitutes the northernmost extension of the East African Rift system. The rift is oriented in the NNE–SSW direction and is bounded by eastern and western plateaus with an average altitude of 2500 m above sea level (m.a.s.l), and its axial zone is characterised by an average altitude of 1600 m.a.s.l [17]. The rift valley and the highlands are characterised by very different climatic conditions. In the rift valley, the climate is semi-arid to arid (the mean annual precipitation is ~650 mm/year, the mean annual temperature is over 20 °C, and the potential evaporation is ~2500 mm/year [17,19,26]), whereas the highlands are humid to sub-humid (the mean annual precipitation is ~1100 mm/year, the mean annual temperature is below 15 °C, and the potential evaporation is ~1000 mm/year [17,19,26]).

The formation of the MER and associated volcanism are related to the Afar mantle plume activity [20–24,41]. During the Oligocene, the region was affected by lithospheric bulging and uplift coupled with extensive continental flood basalt activity [20–24]. Differentiated rhyolite magmas appeared late in the volcano-tectonic evolution of the area, marking the onset of the continental rifting stage [23], which ultimately led to the formation of the East African Rift system [42]. At present, the MER represents an evolved continental rifting basin that is mainly filled by volcanic lithologies, such as silicic tuffs and ignimbrites, and subordinate basaltic lava flows [18,43]. In the MER, the rifting processes have formed various volcano-tectonic depressions, favouring the development of closed lacustrine basins in the rift floor. Rock weathering has also provided clastic particles that were transported and redeposited in fluvio-lacustrine sedimentary facies [18,43]. The MER lakes are subdivided into three groups: (i) Koka, Beseka, Gemeri, and Abe lakes in the northern sector; (ii) Ziway, Langan, Abijata, and Shala lakes in the central sector; and (iii) Awasa, Abaya, and Chamo lakes in the southern sector. The MER lakes are commonly bordered by high-temperature thermal springs, whose occurrence is due to the geothermal circulation of hot fluids, probably due to the persistence of magmatic systems at shallow depths [17].

Because of the high level of evaporation in the rift valley, the water resources in the rift floor (lakes, rivers, and springs) are principally recharged by water derived from the surrounding plateaus [26]. In this framework, the pristine calcium bicarbonate (Ca-HCO_3) water with a low concentration of total dissolved solids (TDS), typical of the basaltic plateau, progressively migrates downhill and reacts with the interacting volcanic lithologies. The weathered rocks release ions to the surface and groundwater, which increases their TDS and pH and drives their evolution toward sodium bicarbonate (Na-HCO_3) hydrochemical facies, typical of the rift valley [16–19,26,44]. Notably, in the rift floor the groundwater is generally in an oxidising condition, with a high potential redox (Eh) and dissolved O_2 , SO_4^{2-} , and NO_3 [19].

3. Materials and Methods

3.1. Sampling

Twenty-nine water samples from lakes and hot and cold springs were collected from the Awasa-Abaya-Chamo lakes district of the MER in January 2012 (Figure 2). Each sampling location was geo-referenced by a portable global positioning system (GPS) (Table 1; Figure 1). Water samples were mainly collected from hot springs bordering the three lakes and along the Bilate River, which feed Abaya Lake. Hot and cold spring samples were also collected inside and/or in the proximity of the following towns: Dimtu, Alaba Kulito (Arto hot springs), and Arba Minch.



Figure 2. Hot and cold spring water sampling sites in the MER collected during field work in January 2012.

Table 1. Sampling localities, geographic coordinates, and physico-chemical parameters of Main Ethiopian Rift (MER) water from lakes and hot and cold springs in the Awasa-Abaya-Chamo lakes district. *T*: temperature; EC: electrical conductivity; TDS: total dissolved solids.

Sample	Latitude	Longitude	Elevation (m)	pH	<i>T</i> (°C)	EC (μS/cm)	TDS (mg/L)	
Awasa Lake and surroundings								
AZ1	06°59'36" N	38°31'19" E	1706	6.2	61	1200	671	Hot spring
AZ2	06°59'27" N	38°31'22" E	1707	6.9	>80	2330	1131	Hot spring
AZ3	07°03'22" N	38°27'27" E	1687	9.9	25	810	574	Lake
AZ17	07°04'46" N	38°38'17" E	1914	7.4	66	1160	573	Hot spring
AZ18	07°04'14" N	38°38'40" E	1912	7.9	59	1120	611	Hot spring
AZ19	07°04'32" N	38°38'33" E	1936	7.7	59	1020	692	Hot spring
Dimtu town								
AZ4	06°56'05" N	38°07'46" E	1489	7.2	37	1030	692	Hot spring
AZ5	06°56'07" N	38°04'46" E	1491	6.9	39	950	666	Hot spring
AZ6	06°56'16" N	38°07'14" E	1491	6.8	39	960	656	Hot spring
AZ11	06°55'41" N	38°08'04" E	1490	8.3	57	1150	745	Hot spring
Bilate River and surroundings								
AZ12	06°48'35" N	38°05'17" E	1346	7.8	45	1340	852	Hot spring
AZ13	06°48'39" N	38°05'13" E	1346	7.5	56	1480	913	Hot spring
AZ14	06°45'18" N	38°02'47" E	1248	7.6	67	5530	3667	Hot spring
AZ15	06°45'22" N	38°02'44" E	1248	7.8	63	5500	3736	Hot spring
AZ16	06°43'22" N	38°02'42" E	1243	7.9	> 80	6200	3722	Hot spring
Abaya Lake and surroundings								
AZ22	06°38'10" N	37°54'34" E	1197	6.6	65	2700	1750	Hot spring
AZ23	06°38'10" N	37°54'35" E	1199	7.3	61	2560	1903	Hot spring
AZ24	06°34'03" N	37°49'30" E	1259	6.4	36	420	280	Hot spring
AZ31	06°14'35" N	37°34'35" E	2682	6.0	17	60	67	Cold spring
AZ32	06°14'29" N	37°34'37" E	2681	5.3	18	10	26	Cold spring
AZ33	06°07'10" N	37°37'46" E	1192	9.1	26	970	799	Lake
Chamo Lake and surroundings								
AZ25	05°53'14" N	37°41'29" E	1116	7.9	40	2270	1770	Hot spring
AZ26	05°53'04" N	37°41'26" E	1136	8.0	46	2400	1734	Hot spring
AZ27	05°53'11" N	37°41'30" E	1126	7.5	45	2450	1779	Hot spring
AZ28	05°53'11" N	37°41'30" E	1125	7.7	56	2600	1757	Hot spring
AZ34	05°55'44" N	37°32'07" E	1121	9.3	29	1640	1225	Lake

Table 1. Cont.

Sample	Latitude	Longitude	Elevation (m)	pH	T (°C)	EC (µS/cm)	TDS (mg/L)	
Arto (near Alba Kulito)								
AZ20	07°18'02" N	38°01'19" E	1797	9.3	74	1930	909	Hot spring
AZ21	07°17'43" N	38°01'11" E	1777	8.9	70	1800	1009	Hot spring
Arba Minch								
AZ29	06°00'13" N	37°33'20" E	1199	7.3	24	300	222	Cold spring

Water temperature (T), pH, and electrical conductivity (EC) were measured directly in the field using a hand-held multiparameter probe (HI9813-5, Hanna Instruments, Ronchi di Villafranca Padovana, Italy) calibrated before sampling. Each water sample was filtered by 0.45 µm filters (Minisart® NML syringe cellulose acetate filters, Sartorius Stedim Biotech GmbH, Goettingen, Germany) and stored in two 100 mL bottles: one for major anion analysis and one acidified with 0.5 mL of concentrated Suprapur HNO₃ for major cation and trace element analyses. Chemical analyses were performed at the Department of Physics and Earth Sciences at University of Ferrara (Italy).

3.2. Analytical Methods

Major anions (F⁻, Cl⁻, Br⁻, NO₃⁻, SO₄²⁻; in mg/L) were analysed by ion chromatography using an ICS-1000 system (Dionex, Waltham, MA USA) calibrated using Dionex “7-ion standard” solutions obtained by different dilutions. Accuracy and precision, based on the repeated analyses of samples and standards, were better than 10% for all the considered parameters. Total alkalinity was determined in water samples using the HI 3811-0 alkalinity test titration kit (Hanna Instruments).

Major cation (Ca²⁺, Mg²⁺, Na⁺, K⁺; in mg/L) and trace element (Li, Rb, Sr, Ba, As, Mo, Cd, Sb, Hg; in µg/L) analyses were carried out by Inductively Coupled Plasma Mass Spectrometry (ICP-MS) using an X Series instrument (Thermo-Scientific, Bremen, Germany) on samples previously diluted 1:10 by deionized Milli-Q water (resistivity of ca. 18.2 MΩ × cm), and known amounts of Re and Rh were introduced as internal standards. During ICP-MS analysis, the potential contribution of isobaric compounds (e.g., ⁴⁰Ar³⁵Cl) formed during the measurement of As (mass 75) was minimised by operating in kinetic energy discrimination (KED) mode, with the collision cell fluxed by a mixture of He–H gas. In each analytical session, the analysis of samples was verified with that of the reference materials EU-L-1 and ES-L1 provided by SCP-Science (www.scpscience.com). Notable, the analyses presented in this work were performed in the same analytical session as other river water samples in which the As concentration was below the detection limit [45], indicating that the significant concentration of As measured in the MER water was not related to systematic analytical interference. Accuracy and precision were determined using several international reference standards and were shown to be lower than 10% of the measured value, with detection limits in the order of 2 µg/L.

Major anions, major cations, and trace elements were also measured on leachates, performed to demonstrate the reactivity of the MER lithologies to natural water. This was done by implementing and refining the approach provided by Rango et al. [16]. Extraction tests were performed by leaching 10 g of volcanic rocks or fluvio-lacustrine sediments with 50 mL of deionized water or Ca–HCO₃ water (Ca²⁺: 12 mg/L, Mg²⁺: 4.4 mg/L, Na⁺: 5 mg/L, K⁺: 5.1 mg/L, HCO₃⁻: 97.6 mg/L, Cl⁻: 5.9 mg/L, F⁻: 0.1 mg/L, SO₄²⁻: 1.4 mg/L); the latter has a composition that simulate the recharge water conveyed from the highlands. The leaching experiments were carried out for 15, 30, and 90 days, and the final leachate solutions were centrifuged at 3000 rpm for 10 min and filtered at 0.45 µm (Minisart® NML syringe cellulose acetate filters) before the analyses.

In particular, the leaching tests were performed on three volcanic rock samples and on two fluvio-lacustrine sediments that were originally investigated by Rango et al. [16,19] through X-Ray fluorescence (XRF) for major and trace elements. The same samples were analysed in this new study to obtain their F⁻ concentrations on powdered samples digested by alkaline fusion following a protocol by [46] (Table S1). Within platinum crucibles, 0.34 g of sample powders were mixed with 0.3 g of KNO₃

and 2 g of Na_2CO_3 and then heated at $1000\text{ }^\circ\text{C}$, thus transforming the contained material in glass. After cooling, crucibles were soaked in beakers containing deionized water, and put in an ultrasonic bath. Solutions were filtered with Whatman 42 filter papers and decanted in 100 mL flasks. Fluoride analyses were done by an Ion Selective Electrode WQ-FL (NexSens, Denver, CO, USA) calibrated with a series of standard solutions of certified F^- content buffered by ionic strength adjuster (ISA) solution, which is used to simulate the pH and ionic content of real samples. Insight into the mineral compositions was obtained with an EVO 50 scanning electron microscope (Zeiss, Jena, Germany) in conjunction with an INCA microanalysis suite (Oxford Instruments, High Wycombe Bucks, UK) (Table S2).

4. Results

4.1. Geochemistry of the MER Natural Water

The physico-chemical characteristics of the MER waters from lakes and hot and cold springs in the Awasa-Abaya-Chamo lakes district are reported in Table 1. Hot spring water samples showed high temperatures varying from $36\text{ }^\circ\text{C}$ to more than $80\text{ }^\circ\text{C}$ (average: $56\text{ }^\circ\text{C}$). The pH values ranged from near neutral to alkaline (range: 6.2–9.3; average: 7.5). The EC varied from $420\text{ }\mu\text{S}/\text{cm}$ to $6200\text{ }\mu\text{S}/\text{cm}$ (average: $2178\text{ }\mu\text{S}/\text{cm}$) and the TDS concentration ranged from 280 to 3736 mg/L (average: 1400 mg/L). Cold spring water samples exhibited lower temperatures (range: $17\text{--}24\text{ }^\circ\text{C}$; average: $20\text{ }^\circ\text{C}$), lower pH values (range: 5.3–7.3; average: 6.2), and lower salinity levels (EC range: $10\text{--}300\text{ }\mu\text{S}/\text{cm}$; average: $123\text{ }\mu\text{S}/\text{cm}$; TDS range: 26–222 mg/L; average: 105 mg/L) than hot spring waters. Lake water samples exhibited medium temperatures (range: $25\text{--}29\text{ }^\circ\text{C}$; average: $26\text{ }^\circ\text{C}$), alkaline pH values (range: 9.1–9.9; average: 9.4), and medium salinity levels (EC_{Awasa L.}: $810\text{ }\mu\text{S}/\text{cm}$; EC_{Abaya L.}: $970\text{ }\mu\text{S}/\text{cm}$; TDS_{Awasa L.}: 574 mg/L; TDS_{Abaya L.}: 799 mg/L), with the exception of Chamo Lake water, which had the highest level of salinity (EC: $1640\text{ }\mu\text{S}/\text{cm}$; TDS: 1225 mg/L). The major ion and trace element compositions of the investigated water are reported in Table 2. On the basis of the relative ion abundance (Table 2), each water sample could be assigned to a hydrochemical facies (Figure 3).

The majority of the MER water sampled in hot springs belongs to Na– HCO_3 hydrochemical facies with concentrations of Na^+ ranging from 53 to 1195 mg/L and HCO_3^- concentrations from 189 to 2241 mg/L. Only the water collected from Chamo hot spring shows sodium sulphate (Na– SO_4) facies composition, having higher concentrations of SO_4^{2-} (930–980 mg/L) with respect to the rest of the investigated hot springs (0–117 mg/L). The water samples collected from the Awasa, Abaya, and Chamo lakes belong to Na– HCO_3 hydrochemical facies with ranges of Na^+ (167–411 mg/L), HCO_3^- (372–600 mg/L), and SO_4^{2-} (2–21 mg/L) similar to those of the majority of hot springs. The water sample from the Arba Minch cold spring and one out of two water samples from the Abaya cold springs displayed Ca– HCO_3 hydrochemical facies (Ca^{2+} : 3–34 mg/L; HCO_3^- : 12–138 mg/L). The other sample from Abaya cold spring had a mixed Ca–Na– HCO_3 composition (Ca^{2+} : 5 mg/L; Na^+ : 8 mg/L; HCO_3^- : 15 mg/L). In general, these compositions are in agreement with those identified in a recent study of MER groundwater sampled along the Bilate River by Haji et al. [40]. In order to assess the risk to human health in relation to the use of the investigated water as drinking water, the relative ion and trace element concentrations were compared with the drinking water quality standards recommended by the authorities: (i) WHO (2011) [3], (ii) European Union (EU–directive 1998 98/83/EC) [47], and (iii) United States Environmental Protection Agency (US EPA–2018 National primary drinking water regulations) [48]. According to the above-mentioned legislation, some investigated water samples displayed SO_4^{2-} , Na^+ , Cd, and Hg concentrations exceeding the respective tolerance thresholds (Table 2). However, the most worrying elements are undoubtedly F^- and As, as the majority of the collected samples were found to have high concentrations of both elements (Table 2; Figures 4a–c and 5a,b). In particular, all water samples from hot springs and lakes had F^- concentrations ranging from 1.5 to 45.2 mg/L, i.e., always higher than the WHO and EU guideline values (F^- : 1.5 mg/L [3,47]), and in many cases, even higher than the EPA tolerance limit, which is less restrictive (F^- : 4 mg/L [48]). Comparably

high F^- concentrations were also recorded in the study of Haji et al. [40]. Some water samples from F^- -contaminated hot springs also had As concentrations exceeding the tolerance limit adopted by all of the legislation considered in this study (As: $10 \mu\text{g/L}$ [3,47,48]). The hot springs along the Bilate River were found to have the most extreme F^- and As concentrations, and in particular, those collected in the proximity of the Abaya lake (AZ14, AZ15, AZ16) exhibited severe F^- and As contamination (F^- : $> 40 \text{ mg/L}$ and As: $> 900 \mu\text{g/L}$; Table 2; Figures 4a–c and 5a,b). Very high F^- and As concentrations were also recorded in other hot springs near the Awasa and Abaya lakes (F^- : $1.5\text{--}18.3 \text{ mg/L}$ and As: $37\text{--}74 \mu\text{g/L}$; Table 2; Figures 4a–c and 5a,b) and in the Arto hot springs (F^- : $27.8\text{--}33.4 \text{ mg/L}$ and As: $31\text{--}41 \mu\text{g/L}$; Table 2; Figures 4a–c and 5a,b). The hot springs near Chamo Lake exhibited high F^- concentrations ($10.9\text{--}11.4 \text{ mg/L}$; Table 2; Figures 4a–c and 5a,b), not correlated with As ($<4\text{--}8 \mu\text{g/L}$; Table 2; Figures 4a–c and 5a,b). Only the water samples from the cold springs had F^- concentrations acceptable for safe drinking-water (F^- : $0.1\text{--}0.6 \text{ mg/L}$; Table 2; Figures 4a–c and 5a,b). Only one out of the three cold spring water samples had enough dissolved As to be measured with our instrument; however, its concentration was well below the tolerance limit (i.e., Arba Minch cold spring: $5 \mu\text{g/L}$; Table 2; Figures 4a–c and 5a,b).

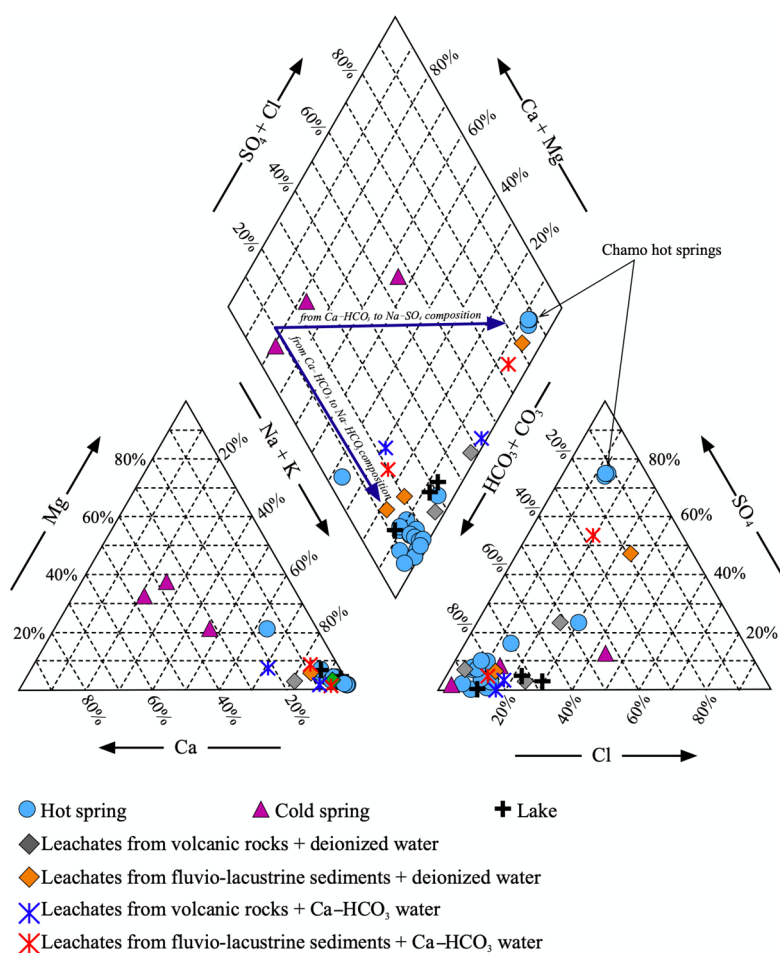


Figure 3. Piper diagram showing the hydrochemical composition of the MER waters from lakes and hot and cold springs in the Awasa-Abaya-Chamo lakes district. The compositions of leachates that simulate water–rock interactions are also reported. Arrows show the water evolution from the highlands (where the Ca-HCO₃ composition dominates) to the rift floor (where the Na-HCO₃ composition prevails).

Table 2. Major ion and trace element compositions of the MER waters from lakes and hot and cold springs in the Awasa-Abaya-Chamo lakes district. Major anions were analysed by Ion Chromatography, whereas major cations and trace elements were analysed by Inductively Coupled Plasma Mass Spectrometry (ICP-MS). n.g.: not given; n.m.: not mentioned.

Sample	Major Ions (mg/L)									Trace Elements (µg/L)								
	F ⁻	Cl ⁻	NO ₃ ⁻	SO ₄ ²⁻	HCO ₃ ⁻	Ca ²⁺	Mg ²⁺	Na ⁺	K ⁺	Li	Rb	Sr	Ba	As	Mo	Cd	Sb	Hg
WHO *	1.5	n.g.	50	n.g.	n.m.	n.g.	n.g.	n.g.	n.g.	n.g.	n.m.	n.m.	700	10	n.g.	3	20	6
EU **	1.5	0.25	50	250	n.m.	n.m.	n.m.	200	n.m.	n.m.	n.m.	n.m.	n.m.	10	n.m.	5	5	n.m.
EPA ***	4	n.m.	10	n.m.	n.m.	n.m.	n.m.	n.m.	n.m.	n.m.	n.m.	n.g.	2000	10	n.g.	50	6	2
Awasa Lake and surroundings																		
AZ1		36.3			444	12.3	5.64	203	15.0	142	75	183	13	37	18	4	<6	<2
AZ2	14.6	73.2		118	600	9.44	3.80	380	25.3	277	130	304	22	74	20	5	7	3
AZ3	9.56	31.1	0.52	1.55	372	8.74	6.38	167	25.2	79	33	100	7	3	12	4	<6	<2
AZ17	1.58	24.7	0.22	0.25	393	5.05	3.92	169	36.1	36	51	96	58	5	14	5	0	<2
AZ18	1.76	27.0	0.12	0.25	429	5.34	3.93	178	38.0	39	50	99	56	7	11	4	<6	<2
AZ19	1.54	24.9	0.14	0.27	426	5.35	4.45	188	41.6	41	54	109	68	<4	12	4	<6	<2
Dimtu town																		
AZ4	15.9	20.2	4.08	26.5	390	4.66	3.52	211	16.4	64	30	47	<5	11	29	<4	<6	<2
AZ5	16.9	17.4	3.66	25.0	387	8.38	3.17	190	14.9	63	34	44	<5	10	32	5	<6	<2
AZ6	17.0	17.7	2.91	25.2	372	6.53	3.50	197	15.1	66	34	43	<5	5	28	<4	<6	<2
AZ11	26.5	36.5	0.33	15.5	420	1.52	0.53	230	14.6	98	19	17	<5	17	36	<4	<6	2
Bilate River and surroundings																		
AZ12	18.4	51.0	0.30	13.3	462	5.49	3.77	282	15.9	99	52	63	20	13	28	<4	<6	2
AZ13	21.0	52.4	0.35	13.7	516	3.11	2.14	291	13.9	131	56	59	45	23	27	<4	<6	<2
AZ14	45.2	147	0.63	73.1	2181	0.46	0.60	1158	60.7	1069	481	283	26	970	13	4	76	27
AZ15	43.5	162		75.2	2241	0.16	0.69	1146	67.6	1024	501	126	14	940	17	6	80	29
AZ16	44.9	144	1.09	72.9	2193	3.34	0.76	1195	67.2	1085	522	289	43	1019	22	8	75	30
Abaya Lake																		
AZ22	18.1	65.5		14.9	1347	6.15	5.70	505	26.9	390	94	108	14	64	17	<4	<6	<2
AZ23	18.3	70.4	0.19	15.9	1542	5.18	6.06	531	28.2	408	94	111	9	54	18	<4	<6	<2
AZ24	2.26	4.43	0.98	0.97	189	11.3	9.04	52.5	9.70	20	18	102	<5	<4	<10	<4	<6	<2
AZ31	0.61	8.56	15.45	3.24	600	4.96	1.90	8.07	9.21	2	6	54	53	<4	<10	<4	<6	<2
AZ32	0.13	1.39	2.64	0.91	0.20	2.99	1.85	2.32	2.26	1	<2	42	20	<4	<10	<4	<6	<2
AZ33	8.97	76.1	0.33	21.3	6.89	12.7	3.58	243	13.4	2	4	130	11	<4	28	<4	<6	<2

Table 2. Cont.

Sample	Major Ions (mg/L)								Trace Elements (µg/L)									
	F ⁻	Cl ⁻	NO ₃ ⁻	SO ₄ ²⁻	HCO ₃ ⁻	Ca ²⁺	Mg ²⁺	Na ⁺	K ⁺	Li	Rb	Sr	Ba	As	Mo	Cd	Sb	Hg
Chamo Lake and surroundings																		
AZ25	10.9	116		954	225	21.1	5.97	430	22.5	494	154	956	4	<4	15	0	<6	<2
AZ26	11.1	115		938	210	14.3	6.22	419	20.2	478	157	961	<5	<4	26	4	<6	<2
AZ27	11.4	118		981	195	25.4	6.43	450	22.4	502	167	1002	<5	8	26	5	<6	<2
AZ28	10.9	115	0.15	930	195	25.4	6.67	441	33.3	491	172	966	11	5	19	4	<6	<2
AZ34	9.33	156	0.13	16.6	600	8.30	9.71	411	15.0	1	3	133	21	<4	29	6	<6	<2
Arto (near Alba Kulito)																		
AZ20	33.4	37.3	0.10	57.5	585	0.00	0.50	309	16.7	177	81	44	<5	41	26	6	2	2
AZ21	27.8	37.1	0.16	57.4	669	0.69	0.64	295	15.5	175	79	104	<5	31	23	2	3	3
Arba Minch																		
AZ29	0.37	3.74	6.39	2.05	138	33.7	14.1	16.8	9.02	1	12	221	<5	5	<10	6	1	<2

WHO * (2011). Guidelines for drinking-water quality [3]. EU ** (1998). Council Directive 98/83/EC of 3rd November 1998 on the quality of water intended for human consumption [47]. EPA *** (2018). National primary drinking water regulations [48].

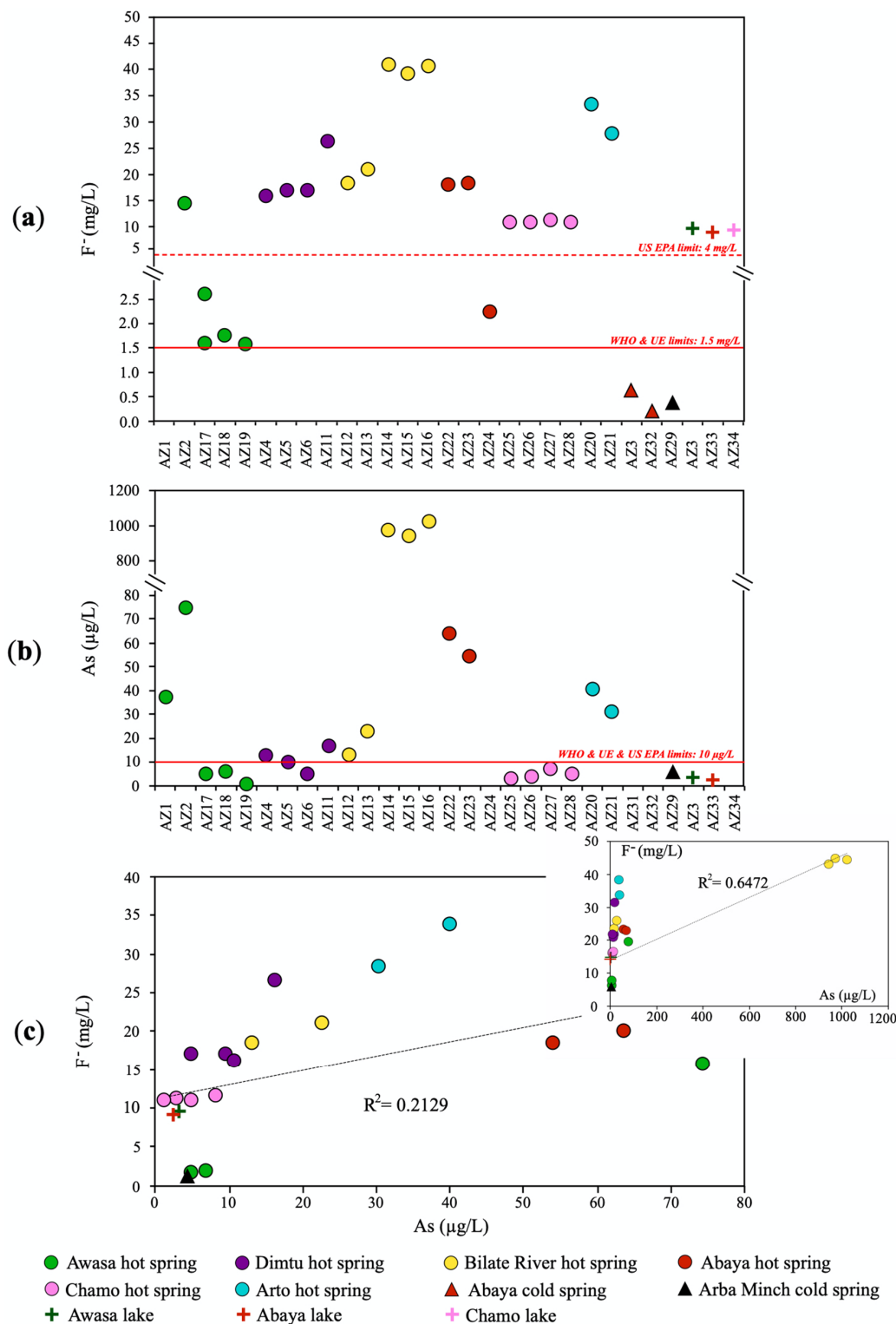


Figure 4. Concentrations of (a) F⁻ and (b) As in the MER lakes and hot and cold springs in the Awasa-Abaya-Chamo lakes district compared with the WHO (2011) [3], EU (1998) [47], and US EPA (2018) [48] guideline values for drinking water. (c) Correlation of F⁻ and As contents in the MER water from lakes and hot and cold springs in the Awasa-Abaya-Chamo lakes district. Note that the correlation lines were calculated using the ordinary least square regression function.

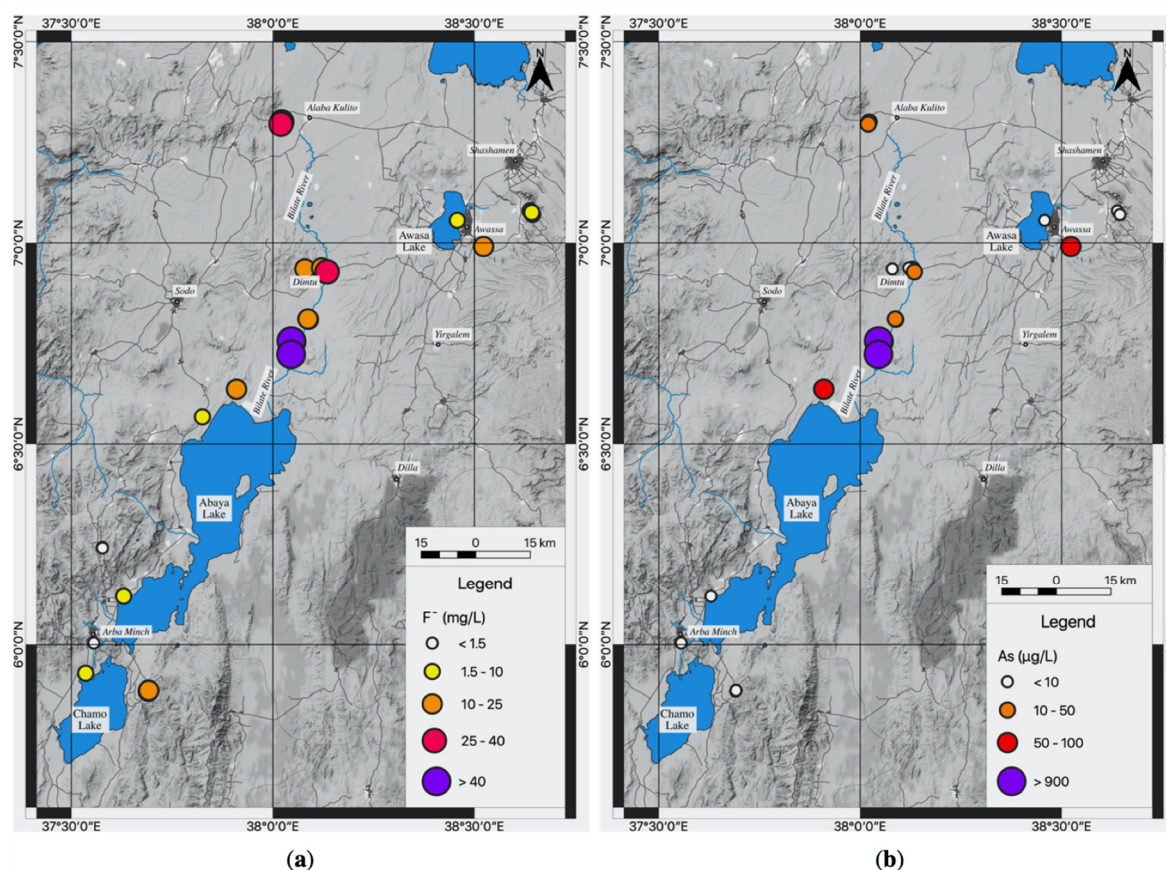


Figure 5. Maps of (a) F^- and (b) As distribution in the MER water from lakes and hot and cold springs in the Awasa-Abaya-Chamo lakes district.

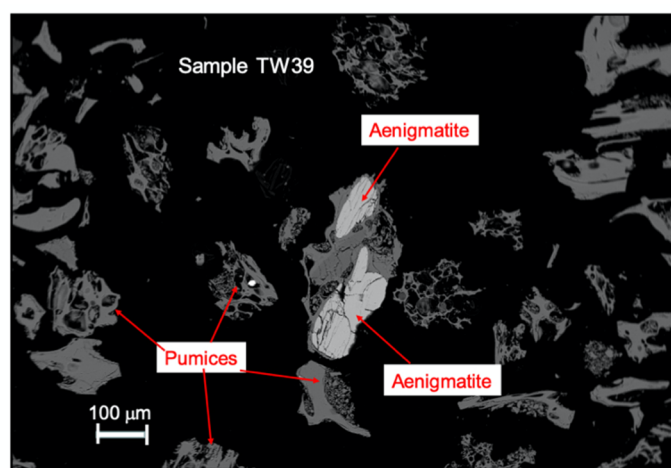
4.2. Geochemistry of the MER Natural Waters

Major and trace element compositions of the investigated MER lithologies are reported in Table S1. The MER volcanic samples (Ted4, TW31, TW39) are pyroclastic deposits with a rhyolitic composition according to their high SiO_2 (71.1–72.1 wt.%) and alkali (6.9–9.6 wt.%) contents (Figure S1a) and low CaO (0.2–0.3 wt.%) and MgO (0.1–0.3 wt.%) contents. They have a peralkaline character, and according to the Al_2O_3 and FeO contents, they can be described as pantellerites (Figure S1b). Fluvio-lacustrine sediments (TW22, Ted38) represent the reworked rhyolitic volcanic deposits and are comparatively depleted in SiO_2 (55.0–61.2 wt.%) and alkali (3.6–5.0 wt.%) and enriched in CaO (5.9–10.3 wt.%), MgO (3.0–5.3 wt.%), and volatile components measured by the loss on ignition (LOI: 9.9–10.3 wt.%).

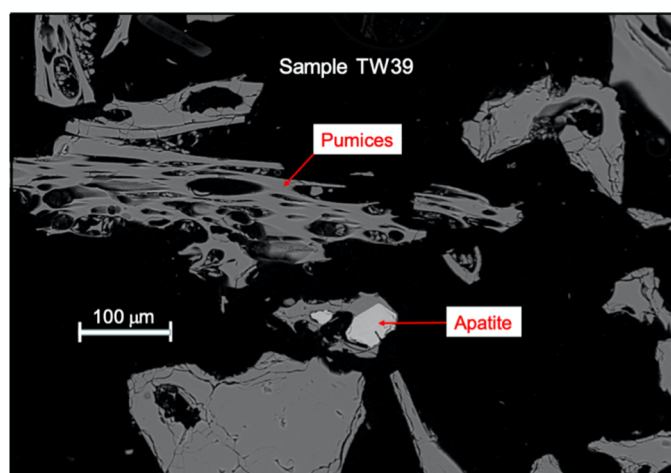
For the trace elements, spider diagrams normalised to the Upper Continental Crust (UCC [49]) composition indicated that some elements (e.g., Ni, Co, Cr, V, Sr, and Pb) showed compatible character during magma differentiation, being depleted with respect to UCC, while others (e.g., REE, Nb, Zr, Zn, and Ga) showed incompatible behaviour and were variously enriched with respect to the UCC (Figure S1c). Our data showed a fluorine (F) content ranging from 985 to 1690 ppm in rhyolitic volcanics, and from 1590 to 2510 ppm in fluvio-lacustrine sediments; thus, they are enriched with respect to UCC (average F_{UCC} : 557 ppm [49]). Arsenic (measured in the MER volcanic rocks and their weathered sediments by Rango et al. [19]) varied from 1.13 to 3.50 ppm in rhyolites and from 1.42 to 16.10 ppm in fluvio-lacustrine sediments; the latter was significantly enriched with respect to the UCC (average As_{UCC} : 4.8 ppm [49]).

SEM investigation (Table S2; Figure 6) revealed that the studied lithologies are prevalently composed of volcanic glass as well as mineral phases such as feldspar, subordinate quartz, amphibole, aegirine-augite clinopyroxene, aenigmatite, oxides, and apatite. This mineral assemblage, plausibly

completed by the presence of sulphides, is similar to those observed in other East African Rift volcanic occurrences [50,51]. The composition of the observed minerals in our samples is listed in Table S2. For the aim of our study, it is important to note that F has been detected in glass (generally 0.2–0.3 wt.%; Table S2), amphibole (up to 2.5 wt.%; Table S2), and fluoro-apatite (up to 6.9 wt.%; Table S2). The F content in glass is consistent with that observed in other East African Rift volcanic occurrences [50,51]. Amphibole in terms of major element classification is intermediate between katophorite and richterite, similar to other East African Rift volcanic mineral assemblages [52–55], and its F content is compatible with what is observed in F-rich sialic rocks [56]. On the other hand, in the MER volcanics, apatite is peculiar as it has a britholite component (Ce-enriched) and an extreme F enrichment, generally only associated with ultra-alkaline/carbonatite melts [57,58], but confirmed by other Ethiopian volcanic occurrences [22].



(a)



(b)

Figure 6. Backscattered SEM image of a MER rhyolitic volcanic rock. Vesiculated particles consist of volcanic glass (containing up to 0.4 wt.% of F), whereas the subhedral white crystals are (a) aenigmatite and (b) fluoroapatite (containing up to 6.9 wt.% of F). Analyses of volcanic glass and other F-bearing mineral phases contained in rock matrices are reported in Table S2.

Arsenic, although below the detection limit, should be present as a trace element in the above-mentioned phases as well as in oxides and hydroxides as demonstrated by several authors [10–12,59–61]. According to Rango et al. [19], As in MER waters is composed of predominantly

(over 80%) arsenate (As(V)) rather than arsenite (As(III)) species, suggesting that the groundwater has oxidising conditions.

5. Discussion

5.1. F^- and As Co-Occurrence in MER Water

Both F^- and As are positively correlated with Na^+ , HCO_3^- , Li, Rb, and TDS (Figure S2). The concentrations of these elements coupled with the high salinity of groundwater indicate that they result from water–rock/sediment interaction [10,11,16–19,22]. In the MER, the weathering and leaching processes generate saline groundwater predominantly composed of a Na– HCO_3 hydrochemical facies with an alkaline pH (Table 2; Figure 3). In particular, the water samples from hot springs contain the highest concentrations of major ions and trace elements (Table 2; Figure S2), indicating that the high T enhanced the hydrolysis of aquifer solid matrices, facilitating the mobility of F^- and As into the MER groundwaters.

Almost all leachates obtained by our extraction tests showed a Na– HCO_3 composition with alkaline pH values comparable with those of natural MER water (Tables 3 and 4; Figure 3), confirming that the water–rock/sediment interaction played a crucial role in the the water’s compositional evolution. The only exceptions were the extracts of sample TW22, which exhibited a Na– SO_4 composition (Figure 3).

In comparison with the rhyolitic volcanics, the fluvio-lacustrine sediments released the highest concentrations of most elements, including F^- and As, only after 15 days (Tables 3 and 4; Figure 7). In particular, TW22 sediments released the highest amounts of F^- (up to 8.52 mg/L; Table 3) and As (up to 188 μ g/L; Table 4). Therefore, the fluvio-lacustrine sediments are not only the main reservoirs of F^- and As in the MER area but can also easily release F^- and As into the water system in a few days. This suggests that the weathered sedimentary particles are more prone to elemental transfer (included F^- and As) to groundwater than rhyolitic volcanic rocks (Figure 7).

Therefore, the weathering of rhyolitic rocks leads to (i) the production of weathered particles (i.e., fluvio-lacustrine sediments), (ii) an increase of pH of natural water, and (iii) the release of F^- and As, due to the dissolution of volcanic glass hosting these elements (Figure 8). The latter process is facilitated by cation exchange processes that remove Ca^{2+} and release Na^+ into the solution [16]. As a consequence, the precipitation of fluorite (CaF_2) is not favoured, increasing the mobility of F^- into groundwater [16–19]. Accordingly, the Saturation Index (SI), calculated using the code PHREEQC [62], invariably shows that MER water is undersaturated in fluorite, favouring F^- mobilisation. However, the weathering of rhyolitic rocks also implies the formation of secondary minerals, such as clay, oxides, and hydroxides, which can further release F^- and As (Figure 8). Subsequent adsorption-desorption processes are influenced by the pH of the solution. In particular, the desorption rate of As increases in alkaline solutions, especially in arid regions [10–12], like those of the MER area [19]. Therefore, the co-occurrence of F^- and As in the MER groundwaters is due to a combination of factors: (i) the presence of F^- and As-bearing rhyolitic lithologies containing a large amount of volcanic glass, (ii) the leaching by alkaline groundwater, and (iii) the arid climate of the area. In addition, the high rate of evaporation, typical of the arid conditions characterising the MER environment [26], further concentrates F^- and As in the shallower parts of the aquifers [10,11,31], increasing the health-risk for the local population.

Table 3. Major ion and trace element compositions of the MER water leachates obtained by the interaction of volcanic rocks and fluvio-lacustrine sediments (10 g of powder) with deionized water (50 mL). Major ions were analysed by Ion Chromatography and trace elements were analysed by ICP-MS after 15, 30, and 90 days. n.a.: not analysed; n.d.: not detected.

Sample	Ted4			TW31			TW39			TW22			Ted38		
	Pyroclastic Deposit			Pyroclastic Deposit			Pyroclastic Deposit			Fluvio-Lacustrine Sediments			Fluvio-Lacustrine Sediments		
	15 days	30 days	90 days	15 days	30 days	90 days	15 days	30 days	90 days	15 days	30 days	90 days	15 days	30 days	90 days
pH	8.38	8.33	8.02	8.67	8.52	8.45	8.26	7.76	8.10	8.64	7.80	8.33	8.06	8.10	n.a.
EC ($\mu\text{S}/\text{cm}$)	460	401	437	143	170	209	199	219	191	1210	1280	1350	416	455	n.a.
F ⁻ (mg/L)	7.73	7.48	8.93	3.16	3.66	3.66	1.62	1.82	2.35	8.00	8.01	8.52	8.73	7.64	n.a.
Cl ⁻	25.5	24.5	26.7	1.67	7.75	17.7	10.0	23.3	11.9	70.6	70.6	160	17.1	1	n.a.
NO ₃ ⁻	35.4	35.2	35.6	n.d.	0.08	0.05	4.78	6.44	19.9	0.45	0.46	0.94	15.0	16.1	n.d.
SO ₄ ²⁻	33.0	32.3	34.2	0.85	2.80	0.69	4.21	4.25	4.65	300	300	310	12.1	12.4	n.a.
* HCO ₃ ⁻	96	72	27	65	71	96	72	63	55	120	154	46	139	176	n.a.
Ca ²⁺	<0.3	<0.3	<0.3	<0.3	<0.3	2.80	4.79	5.93	4.35	7.18	9.64	10.8	7.61	9.51	4.10
Mg ²⁺	<0.4	<0.4	<0.4	<0.4	<0.4	<0.4	<0.4	0.50	<0.4	1.26	1.65	2.69	1.54	2.12	3.80
Na ⁺	84.3	64.9	74.3	27.0	34.1	44.9	29.8	34.0	31.5	217	225	243	61.9	68.9	108
K ⁺	11.0	16.7	8.71	2.92	4.01	6.00	7.47	8.02	6.32	28.3	30.6	36.7	20.6	24.1	26.9
Li ($\mu\text{g}/\text{L}$)	7	7	16	8	13	22	6	6	9	152	159	218	52	63	70
Rb	18	13	20	3	3	6	11	12	8	18	20	25	12	14	12
Sr	<2	<2	<2	<2	<2	4	12	17	8	61	73	97	83	123	156
Ba	<5	<5	5	6	<5	8	<5	10	5	17	14	15	6	16	5
As	<4	5	7	<4	4	4	<4	<4	5	155	170	187	7	7	<4
Mo	<1	<10	<10	<10	<10	<10	<10	<10	<10	416	419	468	<10	<10	<10
Cd	<4	<4	<4	4	<4	<4	<4	<4	<4	4	<4	<4	<4	<4	<4
Sb	<6	<6	6	<6	<6	<6	<6	7	<6	12	9	7	<6	14	<6
Hg	<2	<2	<2	<2	3	4	<2	<2	<2	17	<2	16	<2	<2	<2

* HCO₃⁻ was not measured but was calculated to reach electro-neutrality.

Table 4. Major ion and trace element compositions of the MER water leachates obtained by the interaction of volcanic rocks and fluvio-lacustrine sediments (10 g of powder) with calcium bicarbonate (Ca–HCO₃) water (50 mL). Major ions were analysed by Ion Chromatography and trace elements were analysed by ICP-MS after 15, 30, and 90 days. n.a.: not analysed; n.d.: not detected.

Sample	Ted4			TW31			TW39			TW22			Ted38		
	Pyroclastic Deposit			Pyroclastic Deposit			Pyroclastic Deposit			Fluvio-Lacustrine Sediments			Fluvio-Lacustrine Sediments		
	15 days	30 days	90 days	15 days	30 days	90 days	15 days	30 days	90 days	15 days	30 days	90 days	15 days	30 days	90 days
pH	8.35	8.55	8.30	8.21	8.00	8.18	7.70	7.76	7.68	8.15	7.86	8.30	8.00	8.10	7.81
EC (µS/cm)	588	483	700	302	323	306	312	308	278	1300	1200	1350	540	565	533
F ⁻ (mg/L)	6.42	6.79	7.79	2.94	3.22	3.53	1.77	1.98	2.41	7.80	7.76	8.24	5.97	6.68	8.26
Cl ⁻	32.3	33.5	36.2	7.33	17.1	8.10	17.4	17.2	18.5	7.97	80.3	78.5	23.8	24.7	23.6
NO ₃ ⁻	34.2	31.1	37.6	0.26	n.d.	0.2	4.60	5.76	20.4	n.d.	n.d.	1.21	15.1	18.0	16.7
SO ₄ ²⁻	34.0	35.1	38.0	2.46	1.96	2.30	6.06	6.24	6.30	290	310	300	14.1	14.8	13.7
* HCO ₃ ⁻	48	63	93	144	161	166	139	127	113	146	201	201	216	242	233
Ca ²⁺	<0.3	<0.3	<0.3	1.19	4.51	4.12	11.9	10.6	11.7	9.10	11.3	12.5	14.3	14.1	15.9
Mg ²⁺	<0.4	<0.4	<0.4	<0.4	0.66	<0.4	2.69	2.01	1.56	2.29	2.86	3.03	3.40	4.65	4.52
Na ⁺	70.4	59.2	86.3	56.7	64.5	62.5	45.1	43.8	44.6	221	246	238	77.3	85.6	81.4
K ⁺	17.9	13.0	21.9	8.68	9.72	9.11	13.5	11.7	12.1	35.8	34.5	38.9	28.8	31.2	30.3
Li (µg/L)	11	14	21	15	17	15	8	7	6	191	191	217	70	95	81
Rb	24	26	32	9	9	9	20	18	16	23	22	27	17	20	18
Sr	2	3	4	5	10	7	47	40	29	90	98	107	178	193	210
Ba	<5	<5	<5	54	<5	5	<5	<5	<5	11	20	13	10	6	8
As	<4	<4	62	<4	<4	<4	4	6	9	145	144	188	8	8	6
Mo	<10	<10	11	<10	<10	<10	<10	<10	<10	454	432	477	<10	10	<10
Cd	<4	<4	<4	<4	<4	<4	<4	<4	<4	<4	<4	<4	<4	<4	<4
Sb	<6	<6	<6	<6	<6	<6	<6	<6	<6	<6	10	<6	<6	<6	<6
Hg	<2	<2	<2	<2	<2	<2	<2	<2	<2	<2	<2	<2	<2	<2	<2

* HCO₃⁻ was not measured but was calculated to reach electro-neutrality.

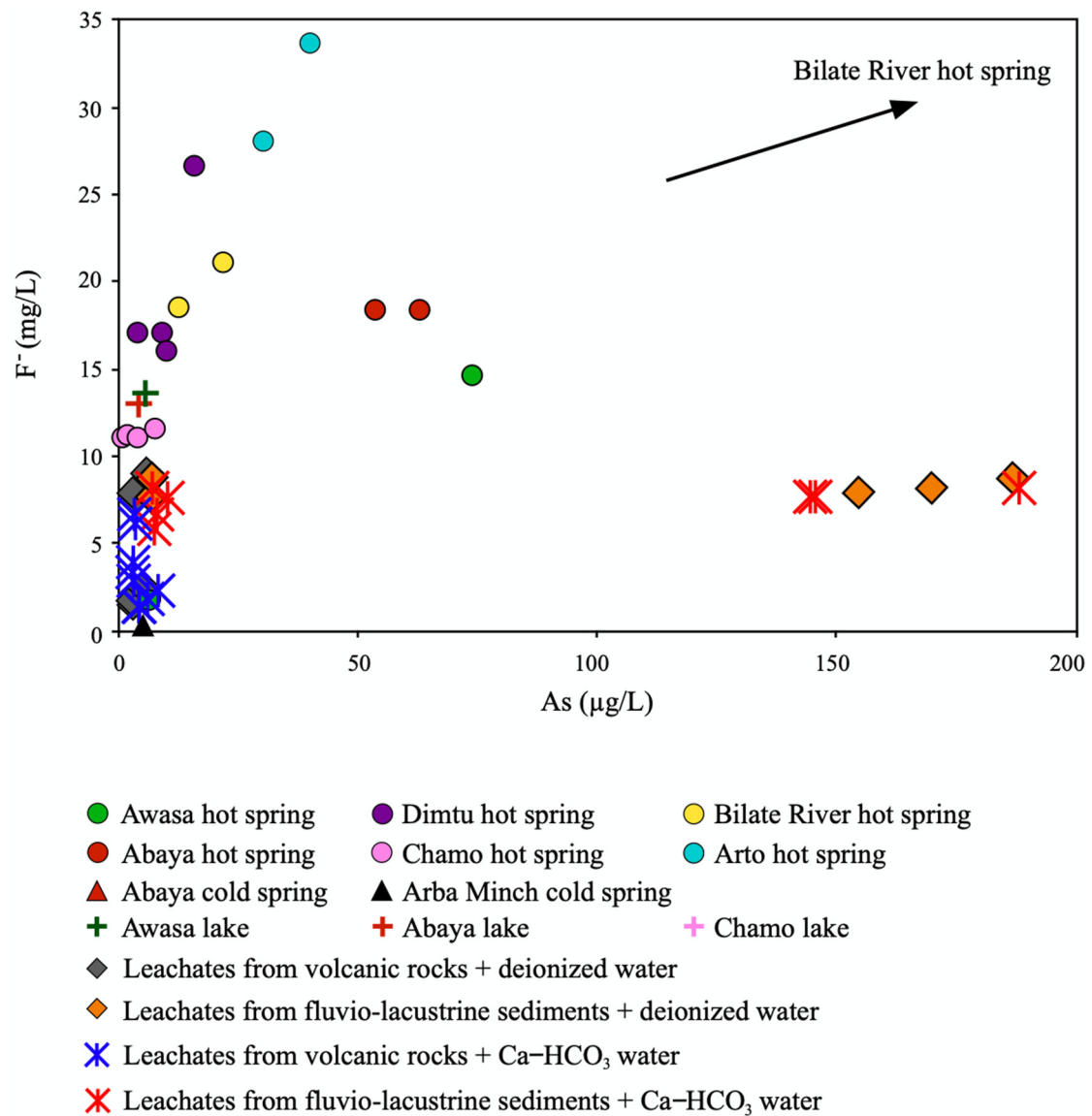


Figure 7. F⁻ vs. As contents of the MER water compared to leachates that simulate the water-rock/sediment interactions with aquifer matrices. Leachates were obtained by the interaction of the MER lithologies with both deionized and calcium bicarbonate (Ca-HCO₃) water.

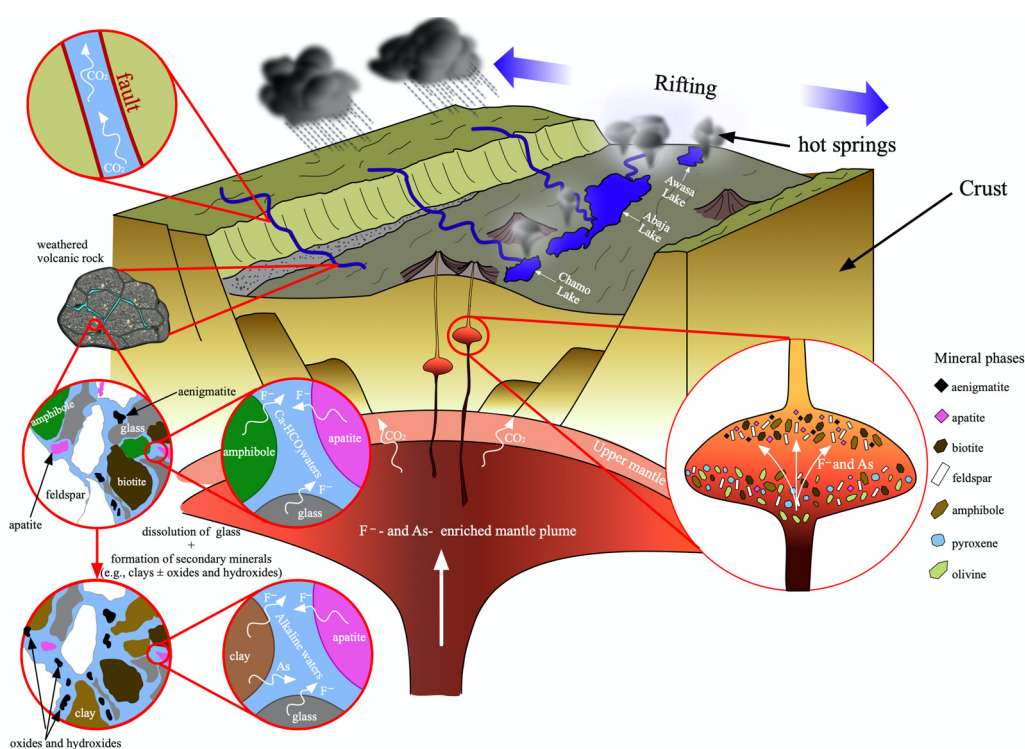


Figure 8. Conceptual model of the geological, geochemical, and environmental processes responsible for the F⁻ and As-enrichment in the MER waters. The processes started with (1) the upraising of a mantle plume enriched in F⁻ and As, which caused the (2) rifting of the area and (3) the eruptions of basic and silicic magmas, which filled the rift valley. (4) During the magmatic differentiation process, F⁻ and As behave as incompatible elements, concentrating in volcanic glass and accessory minerals (e.g., amphibole, biotite, apatite) of differentiated volcanic rocks (i.e., rhyolites). (5) The weathering of silicic lithologies by Ca–HCO₃ water, typical of the MER highlands, induces (6) the dissolution of silica glass, i.e., the main repository of F⁻ and As, and (7) the formation of secondary phases, such as clay, oxides, and hydroxides, which retain F⁻ and As. (8) Subsequently, interactions between rocks and sediments with alkaline water (rich in dissolved CO₂) further release F⁻ and As, inducing the contamination of groundwaters and lakes.

5.2. Geological Origin of F⁻ and As Co-Occurrence in the MER Water

In order to understand the behaviour of F⁻ in geological cycles, the concentration of F has been studied in the main Earth Reservoirs and compared to the concentration of Cl. Fluorine is ten times more depleted with respect to Cl in the most undifferentiated Earth materials provided by chondrites (Ch; F_{Ch}: 64 mg/kg; Cl_{Ch}: 678 mg/kg [63]). It becomes comparatively enriched in the primitive mantle (PM; F_{PM}: 25 mg/kg; Cl_{PM}: 17 mg/kg [63]), and especially enriched in the Upper Crust (UCC; F_{UCC}: 565 mg/kg; Cl_{UCC}: 370 mg/kg [49]). This means that, among halogens, F has a greater affinity to be sequestered by minerals, whereas Cl more likely escapes into fluid phases, ultimately becoming one of the most prevalent ions in the hydrosphere. In magmatic processes during crystal fractionation, F behaves as an incompatible element, as its concentration progressively increases from primitive magma of mantle origin (e.g., basaltic in composition) to residual magma (e.g., rhyolitic in composition), where F concentrates in late stage accessory phases (e.g., apatite, amphibole, biotite, aenigmatite [64,65]). Tectonic settings also play a role in the concentration of this element, and generally, halogens are expected to have higher concentrations in magma from convergent plate settings (i.e., subduction-related) or in magma generated by the melting of very deep mantle sources activated by upraising plumes [66]. The latter seems to be the case for the MER, as the anomalous F concentration in silicic rocks characterises the whole East African Rift, where magma is plausibly related to plume-related mantle sources enriched in halogens (Figure 8). In the studied volcanic

rock, although high F^- contents have been recorded in amphibole and fluoro-apatite, the main F^- repository is the volcanic glass that often constitutes up to 90% of the studied matrices. Glassy particles are highly reactive, and during weathering, they are replaced by clay minerals and amorphous and cryptocrystalline compounds (allophane, imogolite, halloysite), having a remarkable capacity to retain F^- until the leaching of alkaline groundwaters induces its subsequent release (Figure 8) [10,11,67,68]. A similar consideration can be made for As, whose enrichment in the hydrosphere often mirrors that of F^- [10,11]. In fact, the cycling of this element is strongly constrained by the tectonic setting: As is classically associated with subduction-related magmas; however, it is also concentrated in volcanic areas related to upraising plumes, as recorded throughout the whole East African Rift [15] (Figure 8).

Like F^- , during magmatic processes and crystal fractionation, As has incompatible behaviour, being finally trapped in residual silic rocks [13] (Figure 8). In these rocks, As is contained in the same F^- repositories, i.e., volcanic glass [10–13,27–30,69], amphibole, and apatite [70]. Coherently arsenate–phosphate hydroxyapatite solid solution $[Ca_5(P_xAs_{1-x}O_4)_3(OH)]$ is well known in the literature [71–73]. Moreover, As can be contained in solid solution, e.g., in aenigmatite [74,75], magnetite [76], and sulphides, which are other typical minerals of the MER rhyolitic volcanics. As indicated for F^- , the weathering transforms the above-mentioned magmatic minerals in a series of amorphous and cryptocrystalline secondary minerals, especially oxides and hydroxides, which have a notable As adsorption capacity [10,19], until alkaline groundwater undergoes active desorption reactions, which release As into the aquifers (Figure 8). For the thorough understanding of the processes, it is also important to consider the MER geological setting, where groundwater circulates in fault zones that convey mantle-derived CO_2 (Figure 8). This is important as endogenic CO_2 enhances the hydrolysis of silic minerals, oxides, and hydroxides, which release F^- and As, as suggested for other rift zones (e.g., in Namibia and Madagascar), where water anomalies have been recorded [33,34].

6. Conclusions

In many parts of Ethiopia, including the Main Ethiopian Rift (MER), groundwater is the major source of drinking water. Understanding the occurrence, distribution, and sources of potential contaminants in groundwater is therefore important to protect the health of the local populations. In the Awasa–Abaya–Chamo lakes area (southern MER), groundwater contains elevated levels of F^- and As, especially in the hot springs. Hot water rich in dissolved CO_2 leaches the rhyolitic volcanic rocks and their weathered products (i.e., fluvio-lacustrine sediments) more efficiently and, subsequently, can contaminate the groundwater aquifers used for drinking in the region. The weathering of rhyolitic volcanic glass, primary mineral phases (i.e., apatites, amphiboles, and aenigmatites), and secondary phases (i.e., clays, oxides, and hydroxides) by the MER alkaline $Na-HCO_3$ groundwater induces the mobilisation of F^- and As into aquifers, which reaches concentrations that are hazardous to human health. The potential risk is even more serious considering that the fluvio-lacustrine sediments, the main reservoirs of F^- and As in the MER area, can release high amounts of these contaminants into the water system in short periods of time (i.e., a few days), as demonstrated in the leaching experiment. This work also revealed that the only safe drinking water with acceptable concentrations of F^- and As is provided by cold springs far from geothermal systems, as cold water is less effective at leaching the host aquifers. From a practical point of view, the presented data are useful for mapping the quality and geochemistry of water in lakes and hot and cold springs in the MER. In fact, it is necessary to discriminate contaminated water sources that have to be avoided from good-quality water supplies that the locals can access for drinking purposes with the minimal risk to health.

Supplementary Materials: The following are available online at <http://www.mdpi.com/2075-163X/10/5/453/s1>, Figure S1: (a) Total Alkali Silica (TAS [77]) diagram showing the MER volcanic rock and the fluvio-lacustrine sediment composition investigated in this study. Average compositions of rocks studied by Rango et al. [19] are also reported. (b) Al_2O_3 vs. FeO diagram proposed by Macdonald [78] showing the MER volcanic rock and fluvio-lacustrine sediment compositions investigated in this study. Average compositions of rocks and fluvio-lacustrine sediments studied by Rango et al. [19] are also reported. (c) Upper Continental Crust-normalised incompatible trace element patterns of the MER volcanic rocks and fluvio-lacustrine sediments investigated in this

study. Average compositions of rocks and fluvio-lacustrine sediment studied by Rango et al. [19]; Figure S2: F and As contents of the MER water correlated with Na^+ , HCO_3^- , Li, and Rb contents and electrical conductivity (EC), total dissolved solids (TDS), and temperature (T) parameters; Table S1: Major and trace element compositions of MER rocks and fluvio-lacustrine sediments determined by X-Ray Fluorescence (XRF); Table S2: Compositions of volcanic glass and mineral phases hosting F of MER volcanic rocks and fluvio-lacustrine sediments were carried out through a scanning electron microscope (SEM) fitted with an energy dispersive X-ray (EDX) detector routinely calibrated for analysis of major elements in silicates. An additional wavelength dispersive X-ray (WDX) detector was specifically used for analysis of F.

Author Contributions: Conceptualization, G.B. and T.R.G.; methodology, C.M., C.N., T.R.G, A.R. and G.M.S.; investigation, V.B., C.M. and C.N., writing—original draft preparation, G.B. and V.B.; writing—review and editing, G.B. and V.B. All authors have read and agreed to the published version of the manuscript.

Funding: This research received no external funding.

Acknowledgments: The authors are grateful to Renzo Tassinari, which is the responsible of XRF and ICP-MS laboratories at the Department of Physics and Earth Sciences at the University of Ferrara. The authors also thank the Editorial Office and three anonymous reviewers for their constructive criticism and suggestions.

Conflicts of Interest: The authors declare no conflict of interest.

References

- Margat, J.; van der Gun, J. *Groundwater around the World: A Geographic Synopsis*, 1st ed.; CRC Press: New York, NY, USA, 2013; p. 376.
- Bretzler, A.; Johnson, A. The geogenic contamination handbook: Addressing arsenic and fluoride in drinking water. *Appl. Geochem.* **2015**, *63*, 642–646. [[CrossRef](#)]
- WHO. *Guidelines for Drinking-Water Quality*, 4th ed.; World Health Organisation: Geneva, Switzerland, 2011; p. 631.
- Karagas, M.R.; Gossai, A.; Pierce, B.; Ahsan, H. Drinking water Arsenic contamination, skin lesions, and malignancies: A systematic review of the global evidence. *Curr Environ. Health Rep.* **2015**, *2*, 52–68. [[CrossRef](#)] [[PubMed](#)]
- Nickson, R.T.; McArthur, J.M.; Ravenscroft, P.; Burgess, W.G.; Ahmed, K.M. Mechanism of arsenic release to groundwater, Bangladesh and West Bengal. *Appl. Geochem.* **2000**, *15*, 403–413. [[CrossRef](#)]
- Smith, A.H.; Lingas, E.O.; Rahman, M. Contamination of drinking water by arsenic in Bangladesh: A public health emergency. *Bull. World Health Organ.* **2000**, *78*, 1093–1103. [[PubMed](#)]
- Hussain, I.; Arif, M.; Hussain, J. Fluoride contamination in drinking water in rural habitations of Central Rajasthan, India. *Environ. Monit. Assess.* **2012**, *8*, 5151–5158. [[CrossRef](#)]
- Amini, M.; Mueller, K.; Abbaspour, K.C.; Rosenber, T.; Afyuni, M.; Møller, K.N.; Sarr, M.; Johnson, A. Statistical modeling of global geogenic fluoride contamination in groundwaters. *Environ. Sci. Technol.* **2008**, *42*, 3662–3668. [[CrossRef](#)]
- Missimer, T.M.; Teaf, C.M.; Beeson, W.T.; Maliva, R.G.; Woolschlager, J.; Covert, D.J. Natural background and anthropogenic arsenic enrichment in Florida soils, surface water, and groundwater: A review with a discussion on public health risk. *Int. J. Environ. Res. Public Health.* **2018**, *15*, 2278. [[CrossRef](#)]
- Alarcón-Herrera, M.T.; Bundschuh, J.; Nath, B.; Nicolli, H.B.; Gutierrez, M.; Reyes-Gomez, V.M.; Nuñez, D.; Martínez-Dominguez, I.R.; Sracek, O. Co-occurrence of arsenic and fluoride in groundwater of semi-arid regions in Latin America: Genesis, mobility and remediation. *J. Hazard. Mater.* **2013**, 960–969. [[CrossRef](#)]
- Alarcón-Herrera, M.T.; Martin-Alarcon, D.A.; Gutiérrez, M.; Reynoso-Cuevas, L.; Martín-Domínguez, A.; Olmos-Márquez, M.A.; Bundschuh, J. Co-occurrence, possible origin, and health-risk assessment of arsenic and fluoride in drinking water sources in Mexico: Geographical data visualization. *Sci. Total Environ.* **2020**, *698*, 1234168. [[CrossRef](#)]
- Bhattacharya, P.; Claesson, M.; Bundschuh, J.; Sracek, O.; Fagerberg, J.; Jacks, G.; Thir, J.M. Distribution and mobility of arsenic in the Río Dulce alluvial aquifers in Santiago del Estero Province, Argentina. *Sci. Total Environ.* **2006**, *358*, 97–120. [[CrossRef](#)]
- Barringer, J.L.; Reilly, P.A. Arsenic in groundwater: A summary of sources and the biogeochemical and hydrogeologic factors affecting arsenic occurrence and mobility. In *Current Perspectives in Contaminant Hydrology and Water Resources Sustainability*; Paul, B., Ed.; InTechOpen: London, UK, 2013; pp. 82–116. [[CrossRef](#)]

14. Bundschuh, J.; Maity, J.P. Geothermal arsenic: Occurrence, mobility and environmental implications. *Renew. Sustain. Energy Rev.* **2015**, *42*, 1214–1222. [[CrossRef](#)]
15. Mukherjee, A.; Gupta, S.; Coomar, P.; Fryar, A.E.; Guillot, S.; Verma, S.; Bhattacharya, P.; Bundschuh, J.; Charlet, L. Plate tectonics influence on geogenic arsenic cycling: From primary sources to global groundwater enrichment. *Sci. Total Environ.* **2019**, *683*, 793–807. [[CrossRef](#)] [[PubMed](#)]
16. Rango, T.; Bianchini, G.; Beccaluva, L.; Ayenew, T.; Colombani, N. Hydrogeochemical study in the main Ethiopian Rift: New insights to source and enrichment mechanism of fluoride. *J. Environ. Geol.* **2009**, *58*, 109–118. [[CrossRef](#)]
17. Rango, T.; Bianchini, G.; Beccaluva, L.; Tassinari, R. Geochemistry and water quality assessment of central main Ethiopian Rift natural waters with emphasis on source and occurrence of fluoride and arsenic. *J. Afr. Earth Sci.* **2010**, *57*, 479–491. [[CrossRef](#)]
18. Rango, T.; Petrini, R.; Stenni, B.; Bianchini, G.; Slejko, F.; Beccaluva, L.; Ayenew, T. The dynamics of central main Ethiopian Rift waters: Evidence from δD , $\delta^{18}O$ and $^{87}Sr/^{86}Sr$ ratios. *Appl. Geochem.* **2010**, *25*, 1860–1871. [[CrossRef](#)]
19. Rango, T.; Vengosh, A.; Dwyer, G.; Bianchini, G. Mobilization of arsenic and other naturally occurring contaminants in groundwater of the Main Ethiopian Rift aquifers. *Water Res.* **2013**, *47*, 5801–5818. [[CrossRef](#)]
20. Beccaluva, L.; Bianchini, G.; Natali, C.; Siena, F. Continental flood basalts and mantle plumes: A case study of the northern Ethiopian plateau. *J. Petrol.* **2009**, *50*, 1377–1403. [[CrossRef](#)]
21. Beccaluva, L.; Bianchini, G.; Ellam, R.M.; Natali, C.; Santato, A.; Siena, F.; Stuart, F.M. Peridotite xenoliths from Ethiopia: Inferences about mantle processes from plume to rift settings. *GSA Spec. Pap.* **2011**, *478*, 77–104. [[CrossRef](#)]
22. Natali, C.; Beccaluva, L.; Bianchini, G.; Siena, F. Rhyolites associated to Ethiopian CFB: Clues for initial rifting at the Afar plume axis. *Earth Planet. Sci. Lett.* **2011**, *312*, 59–68. [[CrossRef](#)]
23. Natali, C.; Beccaluva, L.; Bianchini, G.; Savo, A.; Ellam, R.M.; Siena, F.; Stuart, F.M. High-MgO lavas associated to CFB as indicators of plume-related thermochemical effects: The case of ultra-titaniferous picrite–basalt from the Northern Ethiopian–Yemeni Plateau. *Gondwana Res.* **2016**, *34*, 29–48. [[CrossRef](#)]
24. Natali, C.; Beccaluva, L.; Bianchini, G.; Siena, F. The Axum-Adwa basalt-trachyte complex: A late magmatic activity at the periphery of the Afar plume. *Contrib. Mineral. Petr.* **2013**, *166*, 351–370. [[CrossRef](#)]
25. Arnórsson, S. Arsenic in surface-and up to 90 °C ground waters in a basalt area, N-Iceland: Processes controlling its mobility. *Appl. Geochem.* **2003**, *18*, 1297–1312. [[CrossRef](#)]
26. Belete, A.; Beccaluva, L.; Bianchini, G.; Colombani, N.; Fazzini, M.; Marchina, C.; Natali, C.; Rango, T. Water-rock interaction and lake hydrochemistry in the Main Ethiopian Rift. In *Landscape and landforms of Ethiopia*; Paolo, B., Ed.; Springer: Berlin/Heidelberg, Germany, 2015; pp. 307–321.
27. Nicolli, H.B.; Bundschuh, J.; Blanco, M.d.C.; Tujchneider, O.C.; Panarello, H.O.; Dapeña, C.; Rusansky, J.E. Arsenic and associated trace-elements in groundwater from the Chaco-Pampean plain, Argentina: Results from 100 years of research. *Sci. Total Environ.* **2012**, *429*, 36–56. [[CrossRef](#)] [[PubMed](#)]
28. Armengol, S.; Ayora, C.; Manzano, M.; Bea, S.A.; Martínez, S. The role of loess weathering in the groundwater chemistry of the Chaco-Pampean Plain (Argentina). *J. Hydrol.* **2020**, 124984. [[CrossRef](#)]
29. Bundschuh, J.; Farias, B.; Martin, R.; Storniolo, A.; Bhattacharya, P.; Cortes, J.; Bonorino, G.; Albouy, R. Groundwater arsenic in the Chaco-Pampean Plain, Argentina: Case study from Robles County, Santiago del Estero Province. *Appl. Geochem.* **2004**, *19*, 231–243. [[CrossRef](#)]
30. Vital, M.; Martínez, D.E.; Babay, P.; Quiroga, S.; Clément, A.; Daval, D. Control of the mobilization of arsenic and other natural pollutants in groundwater by calcium carbonate concretions in the Pampean Aquifer, southeast of the Buenos Aires province, Argentina. *Sci. Total Environ.* **2019**, *674*, 532–543. [[CrossRef](#)] [[PubMed](#)]
31. Nicolli, H.B.; Bundschuh, J.; García, J.W.; Falcón, C.M.; Jean, J.S. Sources and controls for the mobility of arsenic in oxidizing groundwaters from loess-type sediments in arid/semi-arid dry climates devidence from the Chaco-Pampean plain (Argentina). *Water Res.* **2010**, *44*, 5589–5604. [[CrossRef](#)]
32. Aullón, A.A.; Schulz, C.; Bundschuh, J.; Jacks, G.; Thunvik, R.; Gustafsson, J.P.; Mörth, C.M.; Sracek, O.; Ahmad, A.; Bhattacharya, P. Hydrogeochemical controls on the mobility of arsenic, fluoride and other geogenic co-contaminants in the shallow aquifers of northeastern La Pampa Province in Argentina. *Sci. Total Environ.* **2020**, *715*, 136671. [[CrossRef](#)]

33. Sracek, O.; Wanke, H.; Ndakunda, N.N.; Mihaljevič, M.; Buzek, F. Geochemistry and fluoride levels of geothermal springs in Namibia. *J. Geochem. Explor.* **2015**, *148*, 96–104. [[CrossRef](#)]
34. Sracek, O.; Rahobisoa, J.J.; Trubač, J.; Buzek, F.; Andriamamonjy, S.A.; Rambeloson, R.A. Geochemistry of thermal waters and arsenic enrichment at Antsirabe, Central Highlands of Madagascar. *J. Hydrol.* **2019**, *577*, 123895. [[CrossRef](#)]
35. Bretzler, A.; Osenbrück, K.; Gloaguen, R.; Ruprecht, J.S.; Kebede, S.; Stadler, S. Groundwater origin and flow dynamics in active rift systems—A multi-isotope approach in the Main Ethiopian Rift. *J. Hydrol.* **2011**, *402*, 274–289. [[CrossRef](#)]
36. Reimann, C.; Bjorvatn, K.; Frengstad, B.; Melaku, Z.; Tekle-Haimanot, R.; Siewers, U. Drinking water quality in the Ethiopian section of the East African Rift Valley, part I: Data and health aspects. *Sci. Total Environ.* **2003**, *31*, 65–80. [[CrossRef](#)]
37. Rango, T.; Kravchenko, J.; Atlaw, B.; McCornick, P.G.; Jeuland, M.; Merola, B.; Vengosh, A. Groundwater quality and its health impact: An assessment of dental fluorosis in rural inhabitants of the Main Ethiopian Rift. *Environ. Int.* **2012**, *43*, 37–47. [[CrossRef](#)] [[PubMed](#)]
38. Rango, T.; Jeuland, M.; Tekle-Haimanot, R.; Shankar, A.; Alemayehu, B.; Assefa, G.; Whitford, G.; Wolfe, A. Bone quality in fluoride-exposed populations: A novel application of the ultrasonic method. *Bone Rep.* **2020**, *12*, 100235. [[CrossRef](#)]
39. Kravchenko, J.; Rango, T.; Akushevich, I.; Atlaw, B.; McCornick, P.G.; Merola, R.B.; Paul, C.; Weinthal, E.; Harrison, C.; Vengosh, A.; et al. The effect of non-fluoride factors on risk of dental fluorosis: Evidence from rural populations of the Main Ethiopian Rift. *Sci. Total Environ.* **2014**, *488–489*, 595–606. [[CrossRef](#)]
40. Haji, M.; Wang, D.; Li, L.; Qin, D.; Guo, Y. Geochemical Evolution of Fluoride and Implication for F⁻ Enrichment in Groundwater: Example from the Bilate River Basin of Southern Main Ethiopian Rift. *Water* **2018**, *10*, 1799. [[CrossRef](#)]
41. Ayalew, D.; Jung, S.; Romer, R.L.; Kersten, F.; Pfänder, J.A.; Garbe-Schönberg, D. Petrogenesis and origin of modern Ethiopian rift basalts: Constraints from isotope and trace element geochemistry. *Lithos* **2016**, *258–259*, 1–14. [[CrossRef](#)]
42. Corti, G. Continental rift evolution: From rift initiation to incipient break-up in the Main Ethiopian Rift, East Africa. *Earth Sci. Rev.* **2009**, *96*, 1–53. [[CrossRef](#)]
43. Benvenuti, M.; Carnicelli, S.; Belluomini, G.; Dainelli, N.; Di Grazia, S.; Ferrari, G.A.; Iasio, C.; Sagri, M.; Ventura, D.; Atnafu, B.; et al. The Ziway–Shala lake basin (main Ethiopian rift, Ethiopia): A revision of basin evolution with special reference to the Late Quaternary. *J. Afr. Earth Sci.* **2002**, *35*, 247–269. [[CrossRef](#)]
44. Kebede, S.; Travi, Y.; Asfawossen, A.; Alemayehu, T.; Ayenew, T.; Tessema, Z. Groundwater origin and flow along selected transects in Ethiopian rift volcanic aquifers. *Hydrogeol. J.* **2008**, *16*, 55–73. [[CrossRef](#)]
45. Natali, C.; Bianchini, G.; Marchina, C.; Knoeller, K. Geochemistry of the Adige River water from the Eastern Alps to the Adriatic Sea (Italy): Evidences for distinct hydrological components and water-rock interactions. *Environ. Sci. Pollut. Res.* **2016**, *23*, 11677–11694. [[CrossRef](#)] [[PubMed](#)]
46. Chao, T.T.; Sanzolone, R.F. Decomposition techniques. *J. Geochem. Explor.* **1992**, *44*, 65–106. [[CrossRef](#)]
47. European Union. Council Directive 98/83/EC of 3rd November 1998 on the quality of water intended for human consumption. *Off. J. Eur. Community* **1998**, *34*, L330/32–L330/54.
48. United States Environmental Protection Agency. National primary drinking water regulations Long Term 1 Enhanced Surface Water Treatment Rule. Final rule. *Fed. Regist.* **2018**, *67*, 1811.
49. Rudnick, R.L.; Gao, S. Composition of the Continental Crust. In *Treatise on Geochemistry*; Holland, H.D., Turekian, K.K., Eds.; Elsevier: Amsterdam, The Netherlands, 2004; pp. 1–64.
50. Macdonald, R.; Bagiński, B.; Leat, P.T.; White, J.C.; Dzierżanowski, P. Mineral stability in peralkaline silicic rocks: Information from trachytes of the Menengai volcano, Kenya. *Lithos* **2011**, *125*, 553–568. [[CrossRef](#)]
51. Macdonald, R.; Bagiński, B.; Ronga, F.; Dzierżanowski, P.; Lustrino, M.; Marzoli, A.; Melluso, L. Evidence for extreme fractionation of peralkaline silicic magmas, the Boseti volcanic complex, Main Ethiopian Rift. *Miner. Petrol.* **2012**, *104*, 163–175. [[CrossRef](#)]
52. Martz, A.M.; Brown, F.H. Chemistry and mineralogy of some Plio-Pleistocene tuffs from the Shugura Formation, Southwest Ethiopia. *Quaternary Res.* **1981**, *16*, 240–257. [[CrossRef](#)]
53. Ayalew, D.; Barbery, P.; Marty, B.; Reisberg, L.; Yirgu, G.; Pik, R. Source, genesis and giant ignimbrite deposits associated with Ethiopian continental flood basalts. *Geochim. Cosmochim. Acta* **2002**, *66*, 1429–1448. [[CrossRef](#)]

54. Ridolfi, F.; Renzulli, A.; Macdonald, R.; Upton, B. Peralkaline syenite autoliths from Kilombe volcano, Kenya Rift Valley: Evidence for subvolcanic interaction with carbonatic fluids. *Lithos* **2006**, *91*, 373–392. [[CrossRef](#)]
55. Marshall, A.S.; Macdonald, R.; Rogers, N.W.; Fitton, J.G.; Tindle, A.G.; Nejbert, K.; Hinton, R.W. Fractionation of peralkaline silicic magmas: The greater Olkaria volcanic complex, Kenya Rift Valley. *J. Petrol.* **2009**, *50*, 323–359. [[CrossRef](#)]
56. Petersen, E.U.; Essene, E.J.; Peacor, D.R. Fluorine end-member micas and amphiboles. *Am. Mineral.* **1982**, *67*, 538–544.
57. Ryabov, V.V.; Simonov, O.N.; Snisar, S.G. Fluorine and chlorine in apatites, micas, and amphiboles of layered trap intrusions of the Siberian Platform. *Russ. Geol. Geophys.* **2018**, *59*, 363–373. [[CrossRef](#)]
58. Anzolin, H.M.; Dani, N.; Remus, M.V.D.; Ribeiro, R.R.; Nunes, A.R.; Vaccari Ruppel, K.M. Apatite multi-generations in the Três Estradas Carbonatite, Southern Brazil: Physical and chemistry meaning and implications to phosphate ore quality. *Braz. J. Geol.* **2019**, *49*, e20180092. [[CrossRef](#)]
59. Nicolli, H.B.; Suriano, J.; Gomez Peral, M.A.; Ferpozzi, L.H.; Baleani, O. Groundwater contamination with arsenic and other elements in an area of the Pampa, province of Cordoba, Argentina. *Environ. Geol. Water Sci.* **1989**, *14*, 3–16. [[CrossRef](#)]
60. Smedley, P.L.; Nicolli, H.B.; Macdonald, D.M.J.; Barros, A.J.; Tullio, O. Hydrogeochemistry of arsenic and other inorganic constituents in groundwaters from La Pampa, Argentina. *Appl. Geochem.* **2002**, *17*, 259–284. [[CrossRef](#)]
61. Benson, T.R.; Coble, M.A.; Rytuba, J.J.; Mahood, G.A. Lithium enrichment in intracontinental rhyolite magmas leads to Li deposits in caldera basins. *Nat. Commun.* **2017**, *8*. [[CrossRef](#)]
62. Parkhurst, D.L.; Appelo, C.A.J. User's guide to PHREEQC (version 2)—A computer program for speciation, batch-reaction, one-dimensional transport, and inverse geochemical calculations. *USGS Water-Resour. Investig. Rep.* **1999**, *99*, 312.
63. McDonough, W.F.; Sun, S.S. The composition of the Earth. *Chem. Geol.* **1995**, *120*, 223–253. [[CrossRef](#)]
64. Fuge, R. On the behaviour of fluorine and chlorine during magmatic differentiation. *Contrib. Mineral. Petrol.* **1977**, *61*, 245–249. [[CrossRef](#)]
65. Cossío, O.; Navarro-Ciurana, D.; Domènech, C.; Canals, À.; Barbieri, M.; Pittalis, D.; Soler, A.; Ghiglieri, G. F-bearing sediments and rocks in the East African Rift: Characterization and evaluation of F release capacity. *Macla Rev. de la Soc. Española de Mineral.* **2019**, *12*.
66. Urann, B.M.; Le Roux, V.; Hammond, K.; Marschall, H.R.; Lee, C.T.A.; Monteleone, B.D. Fluorine and chlorine in mantle minerals and the halogen budget of the Earth's mantle. *Contrib. Mineral. Petrol.* **2017**, *172*, 51. [[CrossRef](#)]
67. Li, J.; Wang, Y.; Zhu, C.; Xue, X.; Quian, K.; Xie, X.; Wang, Y. Hydrogeochemical processes controlling the mobilization and enrichment of fluoride in groundwater of the North China Plain. *Sci. Total Environ.* **2020**, *730*, 138877. [[CrossRef](#)]
68. Mukherjee, I.; Singh, U.M. Fluoride abundance and their release mechanism in groundwater along with associated human health risks in a geologically heterogeneous semi-arid region of east India. *Microchem. J.* **2020**, *152*, 104304. [[CrossRef](#)]
69. Casentini, B.; Pettine, M.; Millero, F.J. Release of Arsenic from volcanic rocks through interactions with inorganic anions and organic ligands. *Aquat. Geochem.* **2010**, *16*, 373–393. [[CrossRef](#)]
70. Mazziotti-Tagliani, S.; Angelone, M.; Armiento, G.; Pacifico, R. Arsenic and fluorine in the Etnean volcanics from Biancavilla, Sicily, Italy: Environmental implications. *Environ. Earth Sci.* **2012**, *66*, 561–572. [[CrossRef](#)]
71. Zhang, X.; Zhu, Y.; Zeng, H.; Wang, D.; Liu, J.; Liu, H.; Qian, M.; Xu, L. Dissolution and solubility of the arsenate–phosphate hydroxylapatite solid solution $[Ca_5(P_xAs_{1-x}O_4)_3(OH)]$ at 25 °C. *Environ. Chem.* **2011**, *8*, 133–145. [[CrossRef](#)]
72. Liu, W.; Mei, Y.; Etschmann, B.; Brugger, J.; Pearce, M.; Ryan, C.G.; Borg, S.; Wykes, J.; Kappen, P.; Paterson, D.; et al. Arsenic in hydrothermal apatite: Oxidation state, mechanism of uptake, and comparison between experiments and nature. *Geochim. Cosmochim. Acta* **2017**, *196*, 144–159. [[CrossRef](#)]
73. Puzio, B.; Manecki, M.; Kwasniak-Kominek, M. Transition from endothermic to exothermic dissolution of Hydroxyapatite $Ca_5(PO_4)_3OH$ –Johnbaumite $Ca_5(AsO_4)_3OH$ solid solution series at temperatures ranging from 5 to 65 °C. *Minerals* **2018**, *8*, 281. [[CrossRef](#)]
74. Moore, P.B. Welshite, $Ca_2Mg_4Fe_3^+Sb_5^+O_2[Si_4Be_2O_{18}]$, a new member of the aenigmatite group. *Mineral. Mag.* **1978**, *42*, 129–132. [[CrossRef](#)]

75. Grew, E.S.; Barbier, J.; Britten, J.; Halenius, U.; Shearer, C.K. The crystal chemistry of welshite, a non-centrosymmetric (P1) aenigmatite-sapphirine-surinamite group mineral. *Am. Mineral.* **2007**, *92*, 80–90. [[CrossRef](#)]
76. Liu, C.H.; Chuang, Y.H.; Chen, T.Y.; Yuan Tian, Y.; Li, H.; Wang, M.K.; Zhang, W. Mechanism of Arsenic Adsorption on Magnetite Nanoparticles from Water: Thermodynamic and Spectroscopic Studies. *Environ. Sci. Technol.* **2015**, *49*, 7726–7734. [[CrossRef](#)] [[PubMed](#)]
77. Le Maitre, R.W.; Streckeisen, A.; Zanettin, B.; Le Bas, M.J.; Bonin, B.; Bateman, P.; Bellieni, G.; Dudek, A.; Efremova, S.; Keller, J.; et al. *Igneous Rocks: A Classification and Glossary of Terms, Recommendations of the International Union of Geological Sciences Subcommission of the Systematics of Igneous Rocks*; Cambridge University Press: Cambridge, UK, 2002.
78. Macdonald, R. Nomenclature and petrochemistry of the peralkaline oversaturated extrusive rocks. *Bull. Volc.* **1974**, *54*, 78–83. [[CrossRef](#)]



© 2020 by the authors. Licensee MDPI, Basel, Switzerland. This article is an open access article distributed under the terms and conditions of the Creative Commons Attribution (CC BY) license (<http://creativecommons.org/licenses/by/4.0/>).